ADVANCED FUNCTIONAL MATERIALS
www.afm-journal.de

Microribbon-Like Elastomers for Fabricating Macroporous and Highly Flexible Scaffolds that Support Cell Proliferation in 3D

*Li-Hsin Han, Stephanie Yu, Tianyi Wang, Anthony W. Behn, and Fan Yang**

Hydrogel-based scaffolds are widely used for culturing cells in three dimensions due to their tissue-like water content and tunable biochemical and physical properties. Most conventional hydrogels lack the macroporosity desirable for efficient cell proliferation and migration and have limited flexibility when subject to mechanical load. Here microribbon-like elastomers that, when photocrosslinked, can form macroporous and highly flexible scaffolds that support cell proliferation in 3D are developed. These microribbons are produced by wet-spinning gelatin solution into microfibers, followed by drying in acetone, which causes asymmetrical collapse of microfibers to form microribbon-like structures. Gelatin microribbons are then modified using methacrylate anhydride to allow further photocrosslinking into 3D scaffolds. The macroporosity and mechanical properties of the microribbon-based scaffold may be tuned by varying wet-spinning rate, drying temperature, choice of drying agent, level of glutaraldehyde crosslinking, and microribbon density. When encapsulated in the microribbon-based scaffold, human adipose-derived stromal cells proliferated up to 30-fold within 3 weeks. Furthermore, microribbons-based scaffold demonstrate great flexibility and can sustain up to 90% strain and 3 MPa stress without failing. The unique mechanical properties of microribbon-based scaffolds make them promising tools for engineering shock-absorbing tissues such as cartilage and intervertebral discs.

1. Introduction

In the recent decade, methods for culturing cells in 3D environments have received growing attention in the field of tissue engineering, as the 3D approaches are shown to induce cellular behaviors that more closely mimic natural, in vivo bioactivities.[1–5] To engineer desired cellular processes and tissue formation, 3D biomimetic scaffolds that incorporates different biochemical, mechanical or architectural cues have been developed with extensive efforts.[5–19] Hydrogel-based scaffolds are widely used for 3D tissue engineering approach due to their tissue-like water content, tunable biochemical properties, and ease for cell encapsulation.[5–11] However, most hydrogel-based scaffolds are in lack of the macroporosity (pores larger than the size of cells) needed for efficient cell proliferation, migration, blood vessel ingrowth, or extracellular matrix (ECM) production.[20] Most hydrogels consist of micron/nanometer-sized mesh which are often too small to facilitate the above bioactivities. Furthermore, hydrogels are often associated with weak mechanical strength, which limits their applications in engineering load-bearing tissues.

Microfibers, in contrast to hydrogels, possess high mechanical strength and are frequently used as the building blocks to create highly porous scaffolds.[12–19] Microfibers can be bonded to form interconnected network that is inherently resilient to stress and deformation. Such network produces a large internal surface area that is amenable for modification to present biochemical cues. The network of microfibers can form macroporosity to provide ample 3D space that facilitates cell proliferation and ECM production. Therefore, various protocols have been developed to fabricate microfiber-based scaffolds, such as macromolecule self-assembly,[12,13] micro-extrusion,[18,19] electrospinning,[14,16,17] and template-assisted microfabrication.[15] Microfibers can then be bonded into a scaffold using solvent or chemical erosion,[15] solvent removal,[16,17,19] or chemical crosslinking.[14,18] However, these methods often involve the use of organic solvents, excess heat, high stress and harsh pH values, which are not cell-friendly. Therefore, cells are often seeded onto microfiber scaffolds after the fabrication process, and left to grow into the microfiber networks over time. Such processes may result in poor cell infiltration and distribution, which limit the applications of microfiber-based scaffolds for engineering tissues with clinically relevant dimensions.

Dr. L.-H. Han, A. W. Behn, Prof. F. Yang
Department of Orthopaedic Surgery
Stanford University
Stanford, CA 94305, USA
E-mail: fanyang@stanford.edu
S. Yu
Program in Human Biology
Stanford University
Stanford, CA 94305, USA
T. Wang, Prof. F. Yang
Department of Bioengineering
Stanford University
Stanford, CA 94305, USA

DOI: 10.1002/adfm.201201212

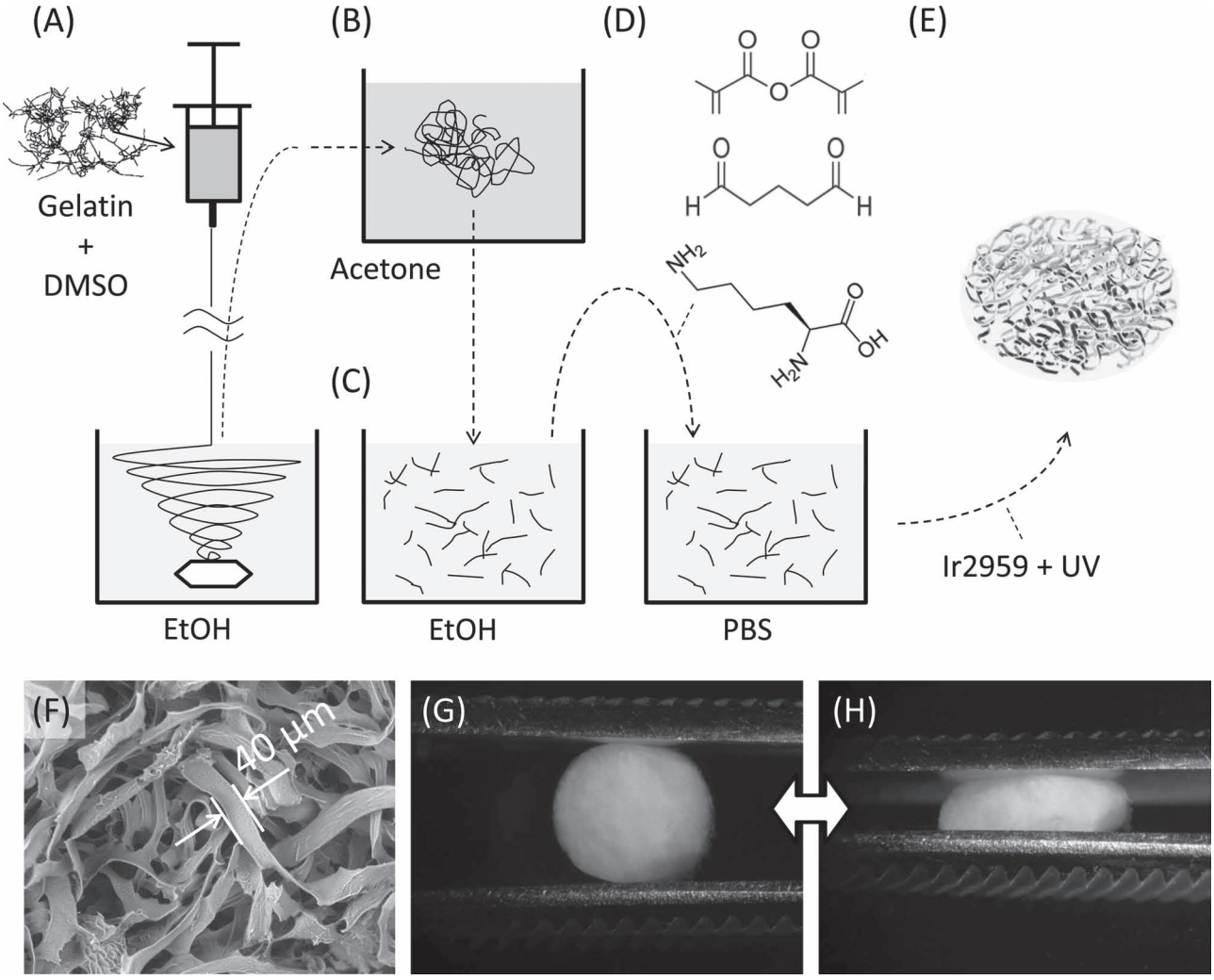

Figure 1. A–E) Schematics of fabrication process of microribbon-based scaffolds. The procedure includes wet-spinning of type-A gelatin (A), solvent drying (B), microribbon dissociation (C), methacrylation and aldehyde fixation (D), and photo-crosslinking (E). F) Scanning electron microscopy shows highly macroporous structure in the resulting microribbon scaffold. G,H) Microribbon-based scaffold showed high flexibility upon compression.

Here we develop microribbon-like, crosslinkable hydrogels for fabricating macroporous and highly flexible tissue engineering scaffolds and investigate their potential for supporting cell culture in 3D. The microribbon-based scaffolds combine the advantages from hydrogel and microfiber-based scaffolds, while overcoming the aforementioned limitations. The microribbons are made from gelatin, which contains abundant ECM cues and widely used for tissue engineering applications.[11,21–23] We examined the effects of fabrication parameters on microribbon properties by varying ejection rate, drying temperature, time of pre-fixation and drying agent, and characterized the resulting scaffold morphology using scanning electron microscopy. The ability of microribbon-based scaffolds to support cell culture was evaluated by quantifying cell spreading, attachment, and proliferation over time. Mechanical property of microribbon-based scaffold was examined using compression test and compared to scaffolds fabricated from microfiber counterparts.

2. Results and Discussion

2.1. Synthesizing Gelatin Microribbons by Wet-Spinning

Our procedure to fabricate the microribbons started with a wet-spinning process of gelatin (**Figure 1**A).We have chosen gelatin, a digested form of collagen, due to its high biomimetic nature and abundance of cell-adhesion sites, which would facilitate cell spreading and migration within the 3D microribbon network. Type-A gelatin (GelA) dissolved in dimethyl sulfoxide (DMSO) was injected from a syringe pump into a bath of anhydrous ethanol with constant stirring. Pulled by gravity and stabilized by a high surface tension, the ejected GelA solution dripped unbrokenly and formed a fine thread, which flowed continuously into the ethanol bath. Since ethanol is a miscible agent to DMSO but an anti-solvent to gelatin, the GelA thread rapidly dried upon contact with ethanol bath and turned into a cluster of microfibers. Constant stirring of ethanol caused a shear flow

Table 1. Different types of microribbons fabricated with varying parameters.

Microribbon Type	Rate of Ejection [mL h^{-1}]	Drying Temperature [°C]	Time of Glutaraldehyde Fixation [h]	Drying Agent
R5-T25-G12-A	5	25	12	acetone
R5-T25-G3-A	5	25	3	acetone
R10-T25-G12-A	10	25	12	acetone
R10-T60-G12-A	10	60	12	acetone
R10-T25-G12-M	10	25	12	methanol

that further narrowed the GelA thread and spun the resulting microfibers into cotton-like bundles.

After the wet-spinning, the microfibers were transferred and dried in acetone bath for 3 h at either 25 °C or 60 °C (Figure 1B). Under both temperatures, drying by acetone caused a rapid and asymmetrical collapse of microfibers, which led to the formation of microribbon structure (Figure 1F). The as-formed microribbons were washed 3-times by ethanol and then dissociated into short segments (<1 mm in length) using a homogenizer (Figure 1C). The microribbons were then treated with methacrylic anhydride, which methacrylated lysines in the microribbons to introduce methacrylate groups onto the microribbon to allow photocrosslinking. To pre-crosslink the microribbons and make them water-insoluble, the methacrylated microribbons were further treated with glutaraldehyde at 40 °C for either 3 or 12 h. The aldehyde-fixed microribbons were finally neutralized by a lysine solution (Figure 1D). Upon exposure to light, the gelatin microribbons crosslinked like hydrogels and formed a macroporous gelatin network (Figure 1E). The resulting scaffold demonstrated a sponge-like physical property and maintained integrity upon squeezing (Figure 1G,H).

2.2. Effects of Fabrication Parameters on Microribbon Properties

The physical and chemical properties of microribbons can be tuned by varying the parameters from fabrication process. The parameters we investigated included the rate of ejection (5 or 10 mL h^{-1}), the temperature for post-spinning drying (25 or 60 °C), the time for glutaraldehyde fixation (3 or 12 h), and the choice of drying agent (acetone or methanol) (**Table 1**).

2.3. Morphology of the Microribbons-Based Scaffolds

To explore the effects of varying microribbon concentration on the morphology of resulting scaffolds, microribbons with increasing densities (2.5, 5, 7.5, and 10% w/v) were photocrosslinked and characterized using scanning electron microscopy (SEM) imaging (**Figure 2**). Upon exposure to light, gelatin microribbons fused into a macroporous scaffold resembling a "highway system" that facilitates cell migration and interactions throughout the whole scaffold. The space among microribbons formed interconnected macroporous channels, which offer ample space for nutrients diffusion, cell proliferation, and matrix production. While increasing microribbon density provides more internal surface area to support cell proliferation, it also reduces the macroporosity of scaffold. The diameter of the interconnected pores is inversely related to the density of microribbons, and increasing the density of microribbons from 2.5 to 10% (w/v) led to a decrease in pore size from about 250 μm to 50 μm. Such change could affect cellular behaviors via altering the curvature of macropore surface that the cells sense.[24] Scaffolds with higher microribbon density also demonstrated more fusion between neighboring microribbons, which further reduced the pore size. Increasing the feeding rate of GelA solution during wet spinning led to wider microribbons. The microribbons produced at 5 mL h^{-1} were 20–50 μm wide (Figure 2A–C), and the ones produced at 10 mL h^{-1} were 60–90 μm wide.

2.4. Effects of Photocrosslinking on Scaffold Volume

Upon photocrosslinking, the microribbons would covalently bind to each other, and led to a decrease in scaffold dimension and volume. The extent of volume shrinkage (quantified by post-crosslinking/original volume × 100%) slightly depended on microribbon density (2.5%: ≈70%, 5%: ≈73%, 10%: ≈77%,) but was almost unaffected by other fabrication parameters, such as feeding rate, degree of aldehyde fixation, or drying temperature for microribbons. Such shrinkage effect should be taken into account when designing the geometry of microribbon-based scaffolds. Once photocrosslinked, the scaffolds remained geometrically stable in PBS at 37 °C, with negligible swelling.

2.5. Cell Spreading and Alignment on Microribbons

To examine whether microribbons support cell culture, human adipose-derived stromal cells (hADSCs) (passage 3) were cultured on dissociated microribbons. Cell morphology and spreading was monitored over time by fluorescence imaging. Two types of microribbons were examined: R10-T25-G12-A and R10-T60-G12-A: the former was dried in acetone at 25 °C and the later at 60 °C (Table 1). Given that proteins tend to unfold secondary and tertiary structures at elevated temperatures,[25,26] we hypothesize that heating at 60 °C would induce changes in the biophysical and biochemical properties of gelatin microribbons, which may lead to different cellular behavior. Fluorescence imaging (**Figure 3**) showed both types of microribbons supported the spreading and growth of hADSCs. Cells started to attach and spread on the microribbons 3 h after cell seeding, and continued to spread and proliferate up to day 16. These

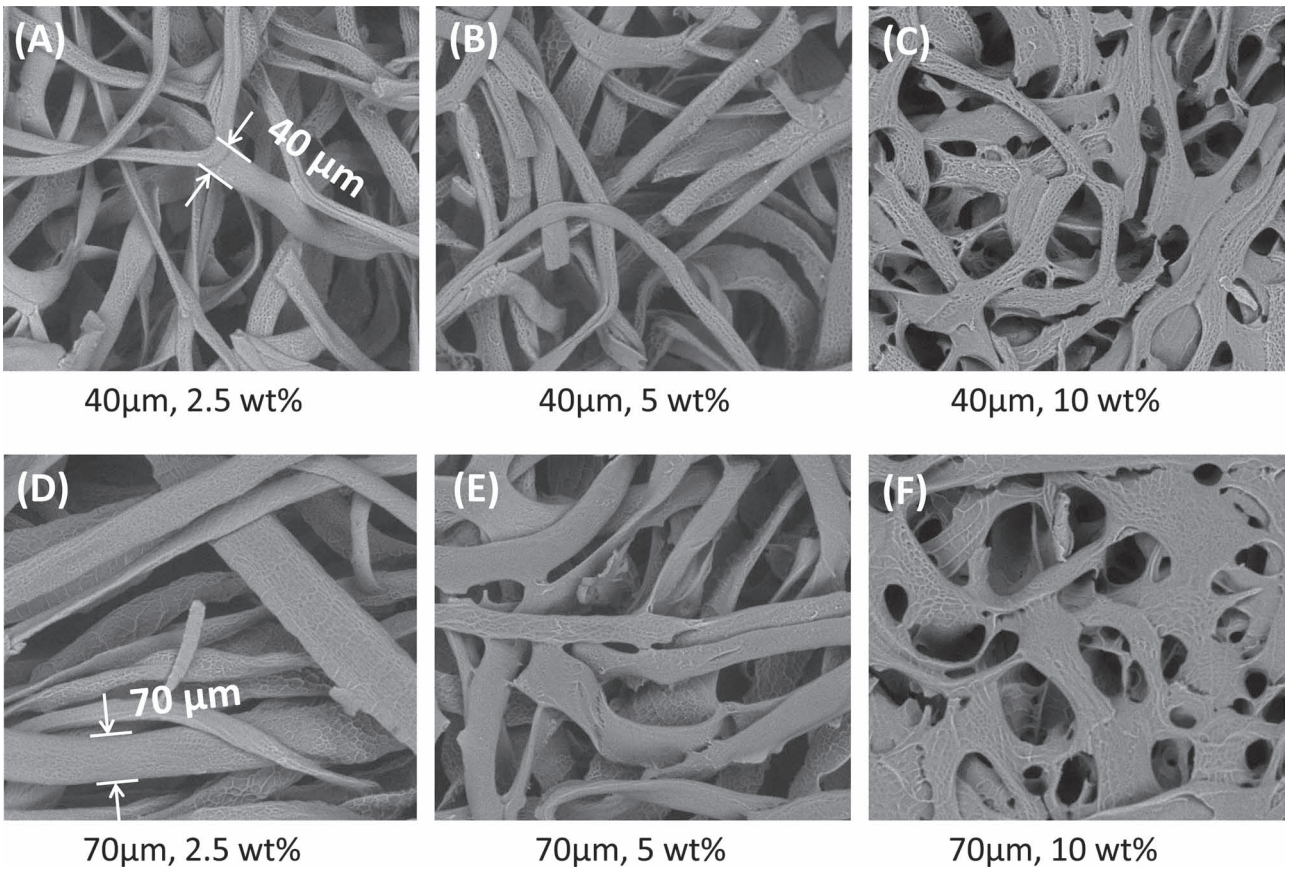

Figure 2. Effects of varying fabrication parameters of microribbon on scaffold morphology. Increasing microribbon concentration (wt%): 2.5% (A,D), 5% (B,E) and 10% (C,F), led to gradually decreased macropore size. Increasing wet-spinning rate from 5 mL h^{-1} (A–C) to 10 mL h^{-1} (D–F) resulted in microribbons with greater width.

results demonstrate that our gelatin microribbons not only facilitate cell encapsulation, but also support cell spreading and proliferation. Furthermore, both types of microribbons (dried at 25 °C or 60 °C) promoted cell alignment along the direction of the microribbons. Elevating drying temperature from 25 °C to 60 °C led to enhanced cell spreading and alignment (n = 300), as shown by the histogram of cell areas (Figure 3G) and the histogram of the alignment angles (Figure 3H) (marked by ∗). One possible explanation for such enhanced cell alignment and spreading on microribbons dried at 60 °C is that heating might promote unfold gelatin molecule and expose more cell-binding sites on the surface of microribbons.

2.6. Cell Proliferation in Photocrosslinked Microribbon Scaffolds in 3D

To evaluate the potential of microribbon-based scaffolds for culturing cells in 3D, hADSCs were encapsulated in photocrosslinked microribbon scaffolds. Cells were mixed with microribbons, and upon exposure to light the microribbons crosslinked into a 3D scaffold with cells distributed throughout the scaffold. Fluorescence imaging demonstrated that microribbon scaffolds are highly supportive for cell proliferation. Cell number increased dramatically over time and reached confluence by day 13 (**Figure 4**).

To further quantify the effects of drying condition on cell proliferation in 3D, two types of microribbons, dried at 25 °C or 60 °C respectively, were used to culture hADSCs. Cell number was quantified using MTS assay over time up to 20 days (**Figure 5**). For each type of microribbon, four groups of scaffolds were fabricated by varying concentration of the microribbons: 2.5, 5, 7.5, and 10% (w/w). Although all groups started with the same cell number at the time of encapsulation (5 million cells per mL), difference in cell number can be detected as early as day 1, with the lowest cell number detected in the groups fabricated with 2.5% (w/v) of microribbons. Scaffolds fabricated using the lowest percentage of microribbon also correlate with highest porosity, which may lead to low seeding efficiency due to cells falling out through the pores before they adhere to the microribbons. Dramatic cell proliferation was observed over time in all groups, and cell number increased up to 30 fold from day 1 to 20.

Cell proliferation in scaffolds with varying microribbon density was comparable overall, with no statistical significance among each other. The cell number in the groups of 2.5 wt% microribbons reached plateau earlier, probably due to the more porosity available for cells to proliferate. Cell proliferation in

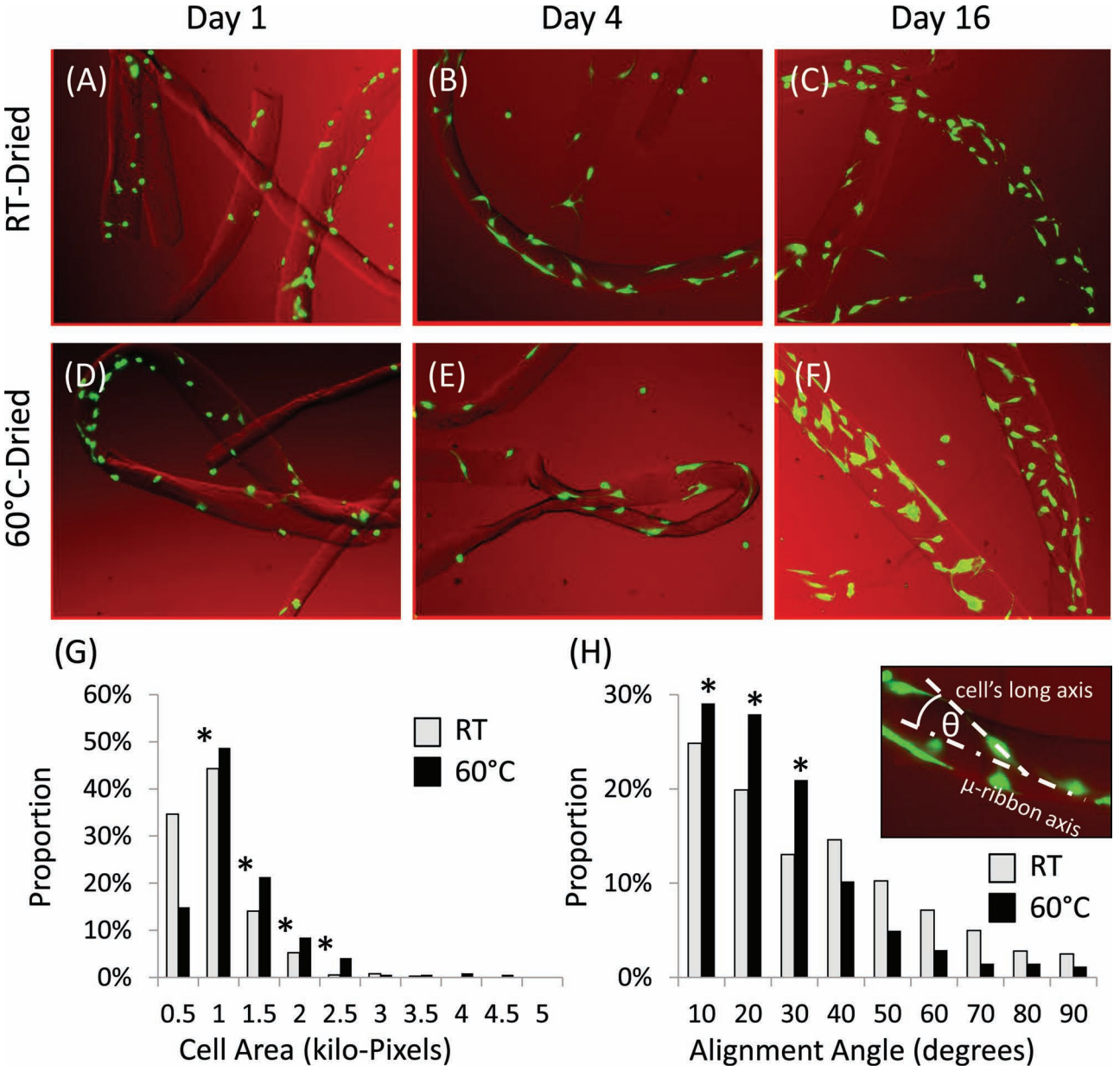

Figure 3. A–F) Spreading, alignment, and proliferation of human adipose-derived stromal cells on the microribbons dried at 25 °C (A–C) and 60 °C (D–F). G,H) Histogram data shows enhanced cell spreading (G) and alignment (H) on microribbons dried at 60 °C than 25 °C (as highlighted by *).

scaffolds of higher microribbon density (7.5 and 10% w/v) demonstrated a continuous increase over time up to day 20. As the microribbon density increases, the resulting scaffolds provide larger internal surface area for cell attachment and proliferation. Meanwhile, increasing microribbon density also decreased the macroporosity, which may also limit cell proliferation. Such counter-balance effects on cell proliferation may explain the comparable total cell number across groups with different microribbon density. Furthermore, cell proliferation increased by 5–20% in microribbons dried at 60 °C compared to their respective controls that were dried at 25 °C. This is consistent with our earlier observation that heated-microribbons promote cell spreading.

2.7. Effect of Microribbon Density on Cell Morphology

Varying microribbon density leads to changed macropore sizes and may affect the cellular behavior via altering the curvature of macropore surface that the cells sense.[24] For example, scaffolds made from 2.5% (w/w) microribbons (**Figure 6**A) had macropores much larger (200–300 μm) than the size of cells, and cells would sense the surface inside the macropores more like a 2D flat surface. For scaffolds made with higher density of microribbons (e.g., 10% (w/w)) (Figure 6C), the macropores became significantly smaller (40–60 μm) and presented a 3D topography to the encapsulated hADSCs. To investigate the effect of microribbon density on cell morphology, hADSCs were encapsulated

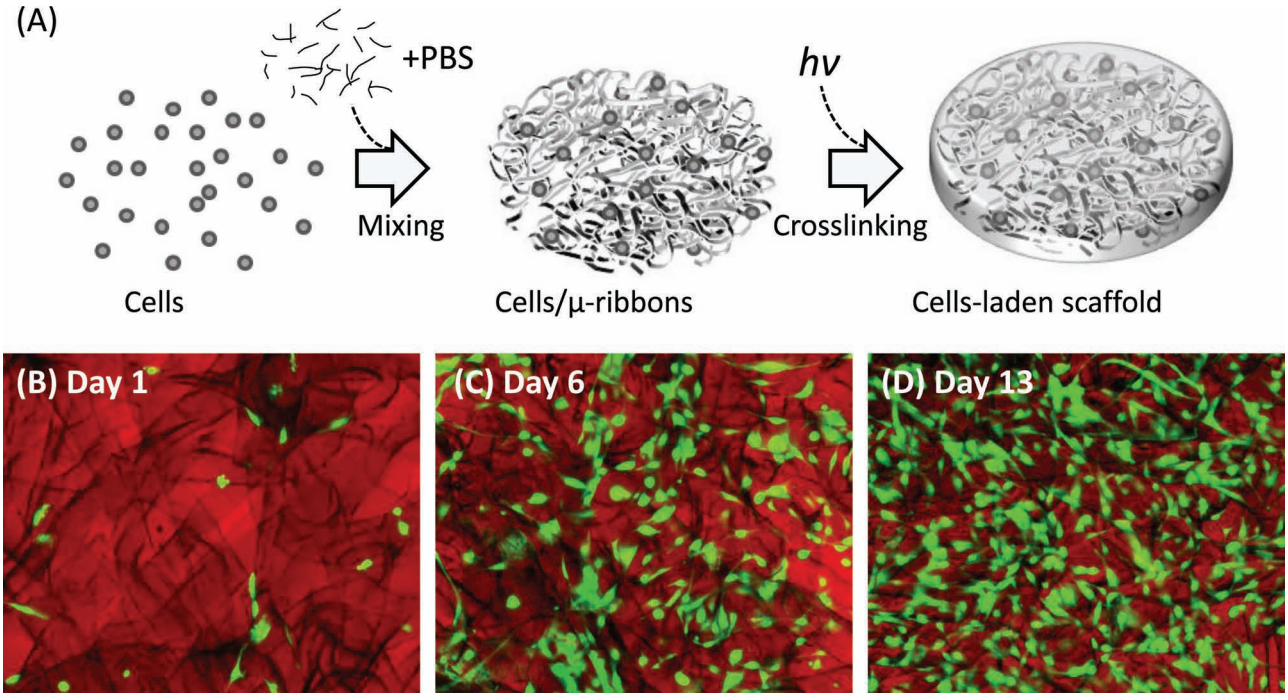

Figure 4. Proliferation of human adipose-derived stromal cells in 3D microribbon-based scaffolds. A) Schematic process of encapsulating cells in photocrosslinkable, microribbon-based scaffolds. B–D) Marked cell proliferation of encapsulated cells in 3D microribbon-based scaffolds over time.

in scaffolds fabricated using varying concentration of microribbons (2.5, 5%, and 10% w/w) (type R10-T25-G12-A), and cell morphology was examined on day 6 and on day 20 (Figure 6). By day 6, cells from all groups proliferated and spread throughout the scaffold network, with no marked difference in cell morphology observed among the groups (Figure 6D–F). By day 20, cell morphology became significantly different, with cells from the 10% group adapting more round-morphology and the cells from the 5% and 2.5% groups adapting more spindle shapes (Figure 6G–I).

Altogether, our results show that microribbons-based scaffolds enable encapsulating cells in 3D and support cell adhesion, spreading and cell proliferation in 3D. The photocrosslinkable microribbon-based scaffolds reported herein combine the strength of traditional hydrogel or microfiber scaffolds while avoiding the associated limitations. The gelatin-based microribbons are highly biomimetic, and its hydrogel-like water content provides a suitable microenvironment for cell culture. Most hydrogel-based scaffolds are associated with nanoscale porosity, which may limit cell proliferation, migration or extracellular

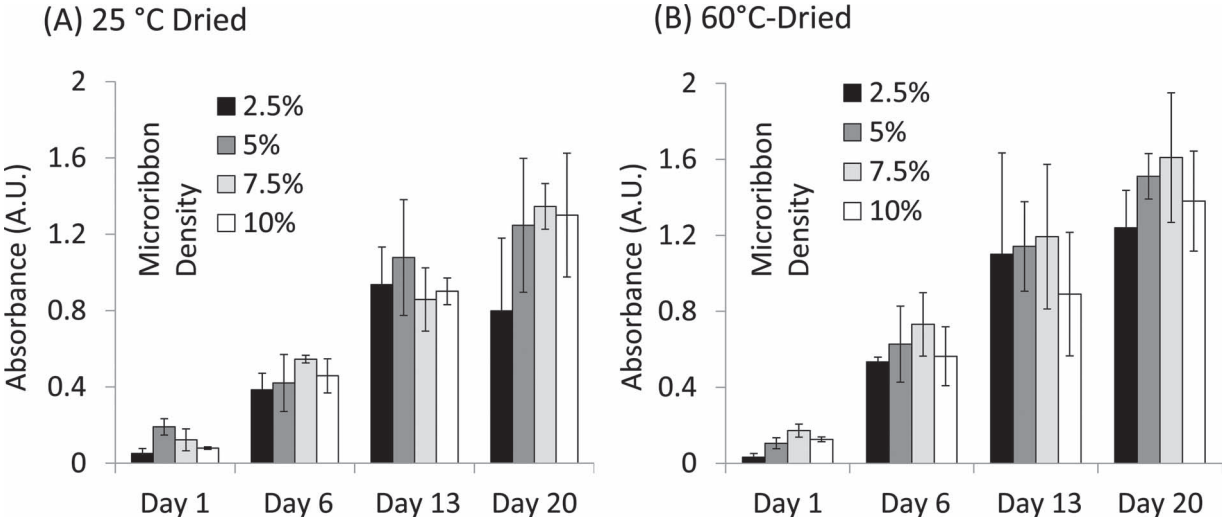

Figure 5. Effects of microribbon density (w/w) and drying temperature on proliferation of human adipose-derived stromal cell in 3D microribbon-based scaffolds over 20 days. A) Quantified cell proliferation in microribbon-based scaffolds dried at 25 °C. B) Quantified proliferation in microribbon-based scaffolds dried at 60 °C. Error bars indicate standard deviations.

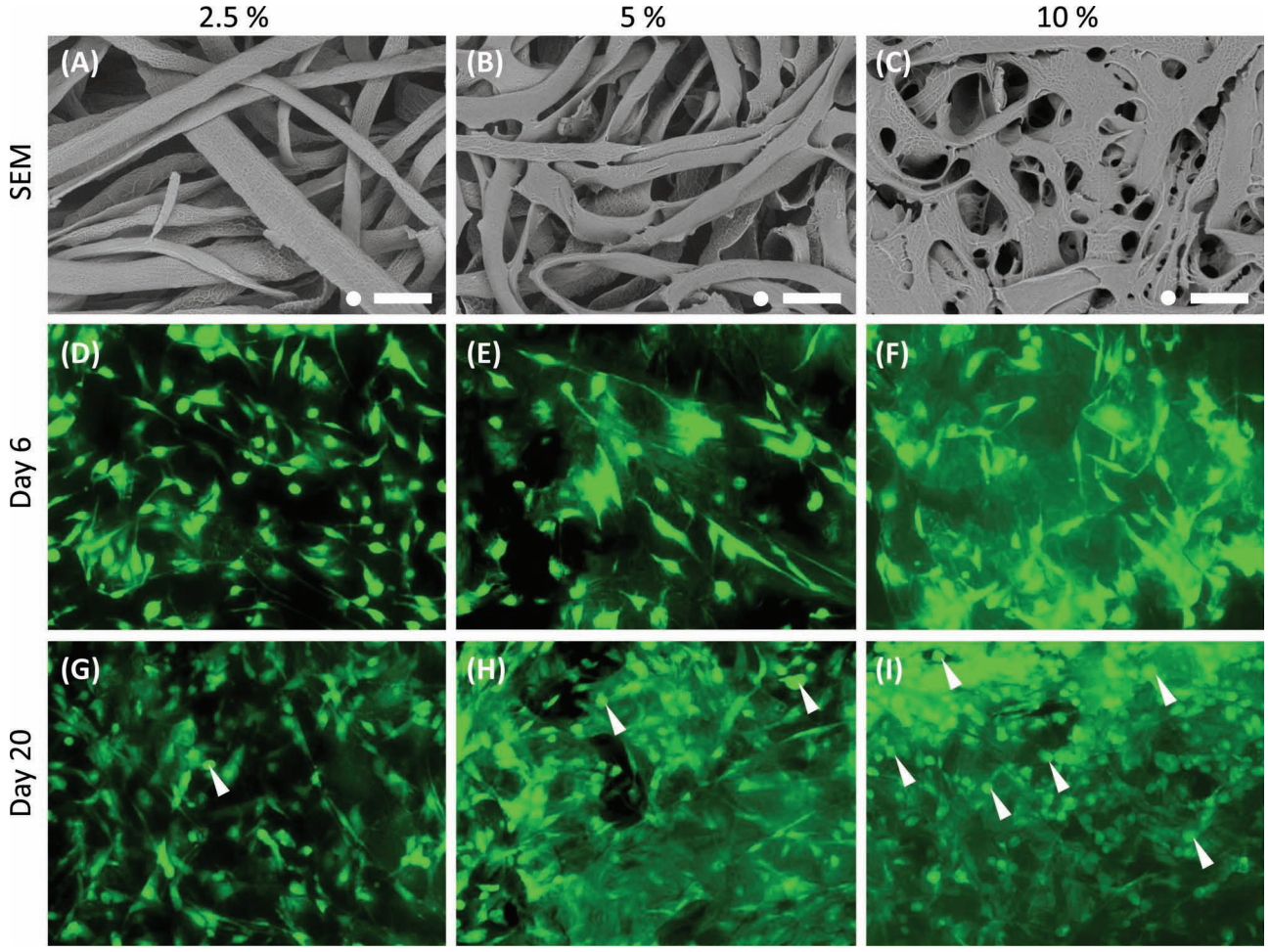

Figure 6. Effects of microribbon density on morphology of hADSCs. A–C) SEM images of scaffolds made by 2.5%, 5%, and 10% microribbons. The scale bars indicate 100 µm and the white dots mark the typical size of hADSC (20 µm). D–F) Calcein AM-labeled hADSCs in microribbon scaffolds on day 6. G–I) Labeled hADSCs in microribbon scaffolds on day 20; the arrow heads selectively mark hADSCs that adapted round morphology.

matrix production. To overcome this problem, macroporosity can be introduced in hydrogels using porogen-leaching process.[27] However, porogen removal procedures may lead to significant loss of mechanical strength of the scaffold, and may sometime cause cytotoxicity depending on the porogen removal stimuli. The photocrosslinked microribbon scaffolds developed here possess large internal surface area and highly interconnected macropores to promote desired cellular processes, while retaining mechanical integrity and flexibility. Furthermore, since the microribbons promote cell alignment, they hold great promise as scaffolds for regenerating tissues with anisotropic nature, such as nerves, muscles, and cardiovascular tissues, in which cell alignment are highly desirable for tissue functions.

2.8. Mechanical Property of Microribbon-Based Scaffolds

Mechanical property is an important aspect of tissue engineering scaffolds, and determines whether the scaffolds can be used for engineering load-bearing tissues such as bone or cartilage. Furthermore, stiffness of the scaffolds themselves provides biophysical cues to directly influence cell fates.[28,29] Compressive modulus measurement was performed to characterize the mechanical property of microribbon-based scaffolds fabricated using varying microribbon width, density, and drying temperature. Increasing the density of microribbons led to a non-linear increase in the stiffness of scaffolds, with a large range of tunable compressive modulus from 0.3 kPa to ≈100 kPa. A small increase in microribbon stiffness was observed when density increased from 2.5% to 5% (w/w), and the overall compressive modulus remained low (≈6 kPa). Further increases in microribbon density to 10% led to over 10–30 fold increase in compressive modulus of the resulting scaffolds compared to their 5% controls. This is likely due to the fact that microribbons fuse with each other to form a stronger network when the density was increased from 5% to 10% (w/w) (Figure 2). Increasing microribbon width from 40 to 70 µm led to a 100% increase in scaffold compressive modulus at high concentration range (10%) (p = 0.013) (**Figure 7**A). Increasing drying temperature to 60 °C led to a slight increase in scaffold modulus at high microribbon concentration (10% w/w), while not much difference was observed at lower microribbon concentration groups (Figure 7B).

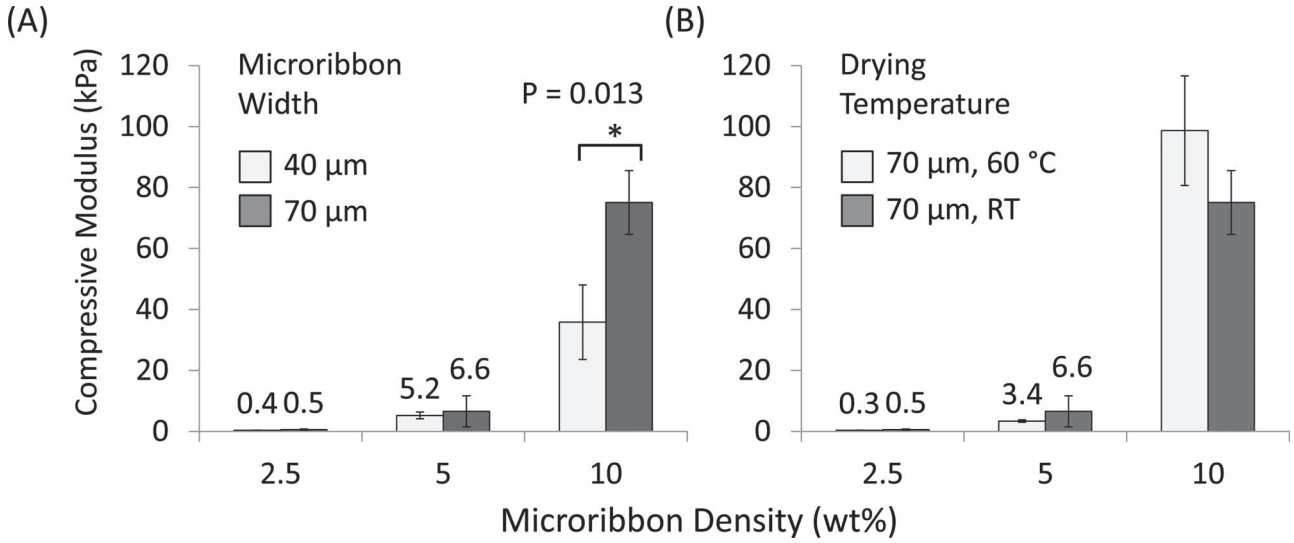

Figure 7. Effect of varying microribbon width, concentration and drying temperature on the stiffness (compressive modulus at 15% strain) of resulting photocrosslinked scaffolds. A) Enhancement of scaffold stiffness by increased average microribbon width (from 40 to 70 µm). B) Enhancement of scaffold stiffness by increased drying temperature (from 25 °C to 60 °C). Note the non-linear enhancement of scaffold stiffness by increased microribbon density (w/w). Error bars indicate standard deviations. $*p < 0.05$.

2.9. Effects of Glutaraldehyde Fixation on Scaffold Morphology and Mechanical Properties

Gelatin is a protein based material and can be crosslinked using glutaraldehyde prior to photocrosslinking. By varying the degree of glutaraldehyde treatment, we can further tune the morphology and mechanical property of the resulting scaffolds. Short glutaraldehyde treatment (3 h) led to partially crosslinked microribbons, which were soluble in water at 37 °C. Increasing glutaraldehyde treatment up to 12 h led to much more stable microribbons, which remain physically stable in water at 37 °C for more than a week. Upon photocrosslinking, 12-h-fixed microribbons maintained their shape while 3-h-fixed microribbons fused with each other with decreased pore size (**Figure 8**A,B). The less-fixed microribbons have higher mobility that allows the methacrylate groups to

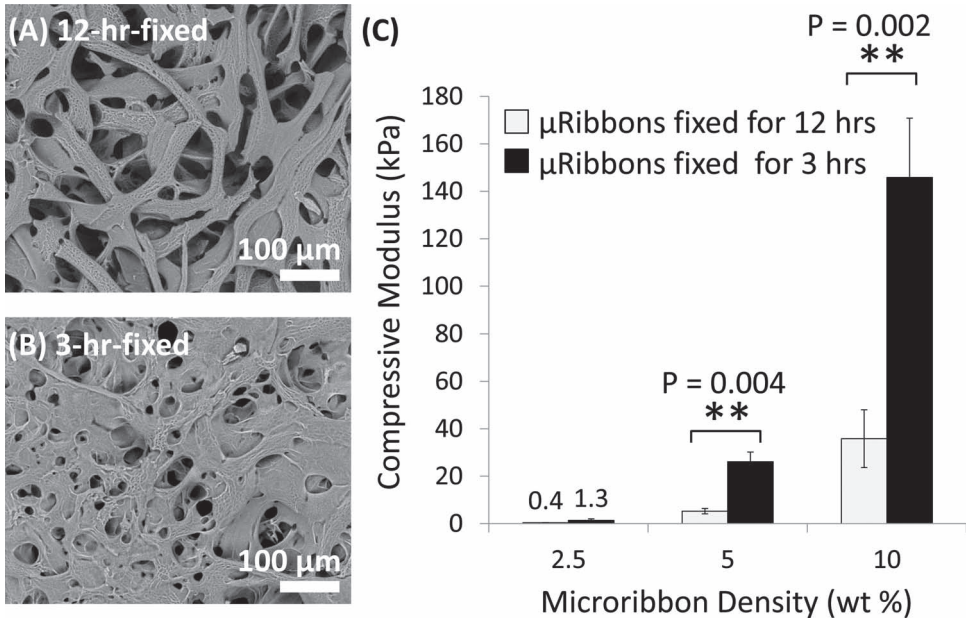

Figure 8. Increased scaffold stiffness (at 15% strain) resulting from decreased aldehyde fixation. A,B) Increased microribbon fusion due to decreased aldehyde fixation (3 h vs 12 h). C) Significantly increased scaffold stiffness (quantified by compression test) due to decreased aldehyde fixation. Error bars indicate standard deviations. $**p < 0.005$.

form stronger inter-crosslinked networks, which led to 3–5 fold increase in mechanical strength of the resulting scaffolds (Figure 8C).

2.10. Decoupling Scaffold Microscopic Stiffness from Bulk Mechanical Strength

One unique advantage of our microribbon-based scaffold is its ability to decouple the "microenvironment stiffness" that the cells sense (determined by the individual microribbon rigidity) from the "scaffold bulk stiffness" (determined by the microribbon density and pore size). This allows independent tuning of the stiffness that cells sense and the bulk scaffold stiffness for different mechanical loading requirement.

2.11. Enhanced Flexibility of Microribbon-Based Scaffolds vs. Microfiber-Based Scaffolds

Unlike the conventional microfibers, the novel microribbons reported here is characterized by the high aspect ratio of cross section, which resembles strip-springs (inset of **Figure 9**A). We hypothesize that such unique microstructures would convey enhanced flexibility and resilience when challenged by mechanical stress. To test our hypothesis, we fabricated two types of scaffolds using either microribbons or microfibers as the building blocks. All the parameters were kept the same except the drying agent, which led to different aspect ratio of cross section. Drying the gelatin fibers in acetone led to a rapid asymmetric collapse and formation of microribbons with flat cross sections (Figure 9A). In contrast, replacing acetone by methanol led to a symmetrical drying, which produced microfibers with round cross sections (Figure 9B). The microfibers shared the same biochemical and surface properties as the microribbons, and formed macroporous scaffolds upon photocrosslinking. Our compressive testing showed dramatically enhanced flexibility in microribbon-based scaffolds compared to the microfiber-based scaffolds. Microribbon-based scaffolds (5% w/w) can be compressed up to 90% strain and instantly reversed to its original shape upon the removal of external force (Figure 9C–F) (also shown by the video in supplementary materials). In contrast, microfiber-based scaffolds (5% w/w) underwent permanent deformation when the compressive strain exceeded 60% (data not shown).

To quantify the flexibility and resilience of microribbon- and microfiber-based scaffolds, we applied cyclic compressions (10 times for each strain) to scaffolds and analyzed the resulting

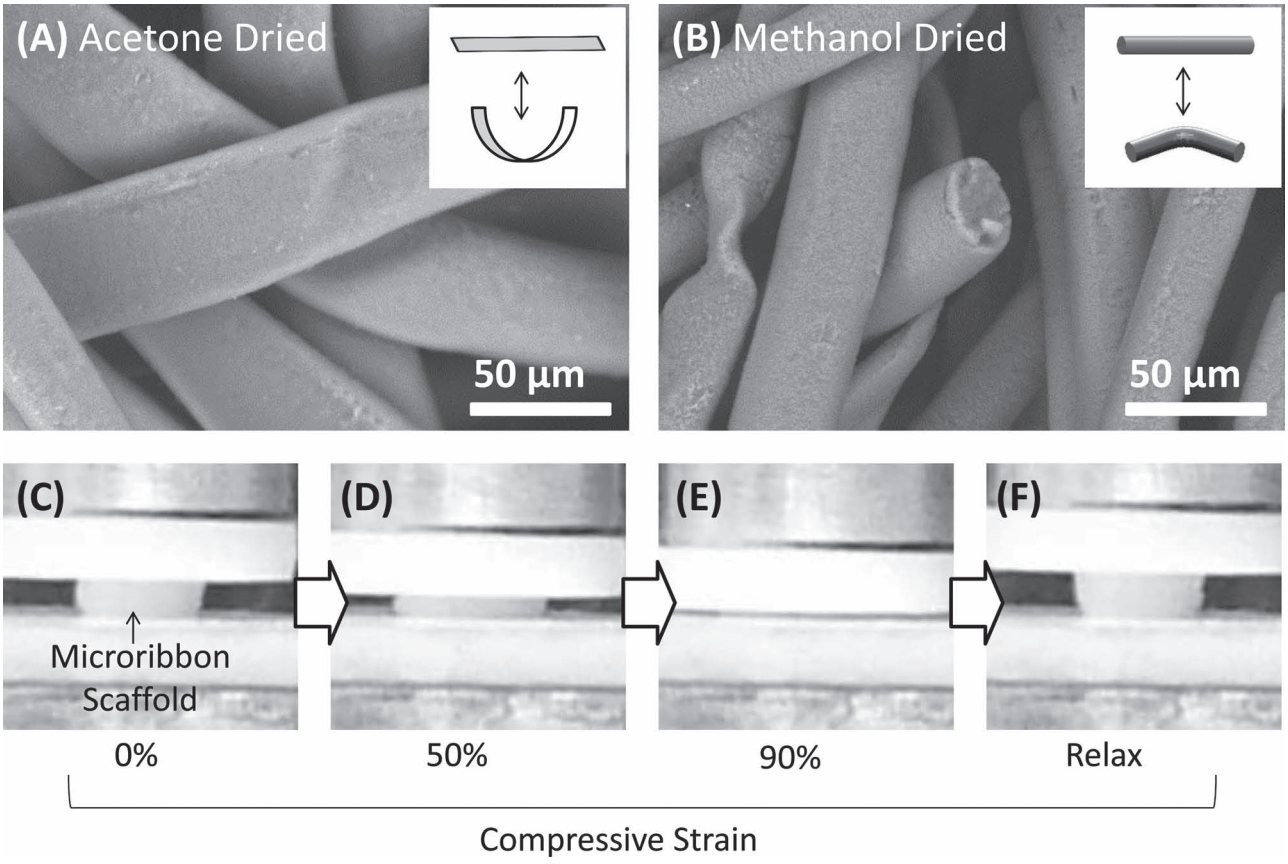

Figure 9. Effect of drying agent on the microribbon cross section and the scaffold flexibility. A) Flat cross section (microribbons) resulting from acetone drying. B) Round cross sections (microfibers) resulting from methanol drying. Insets of (A,B) illustrate the effect of cross-section on the flexibility of microribbons/microfibers. C–F) Exceptional flexibility of microribbon scaffold demonstrated by the compression test of 5 wt% microribbon scaffolds (from 0 to 90% compression).

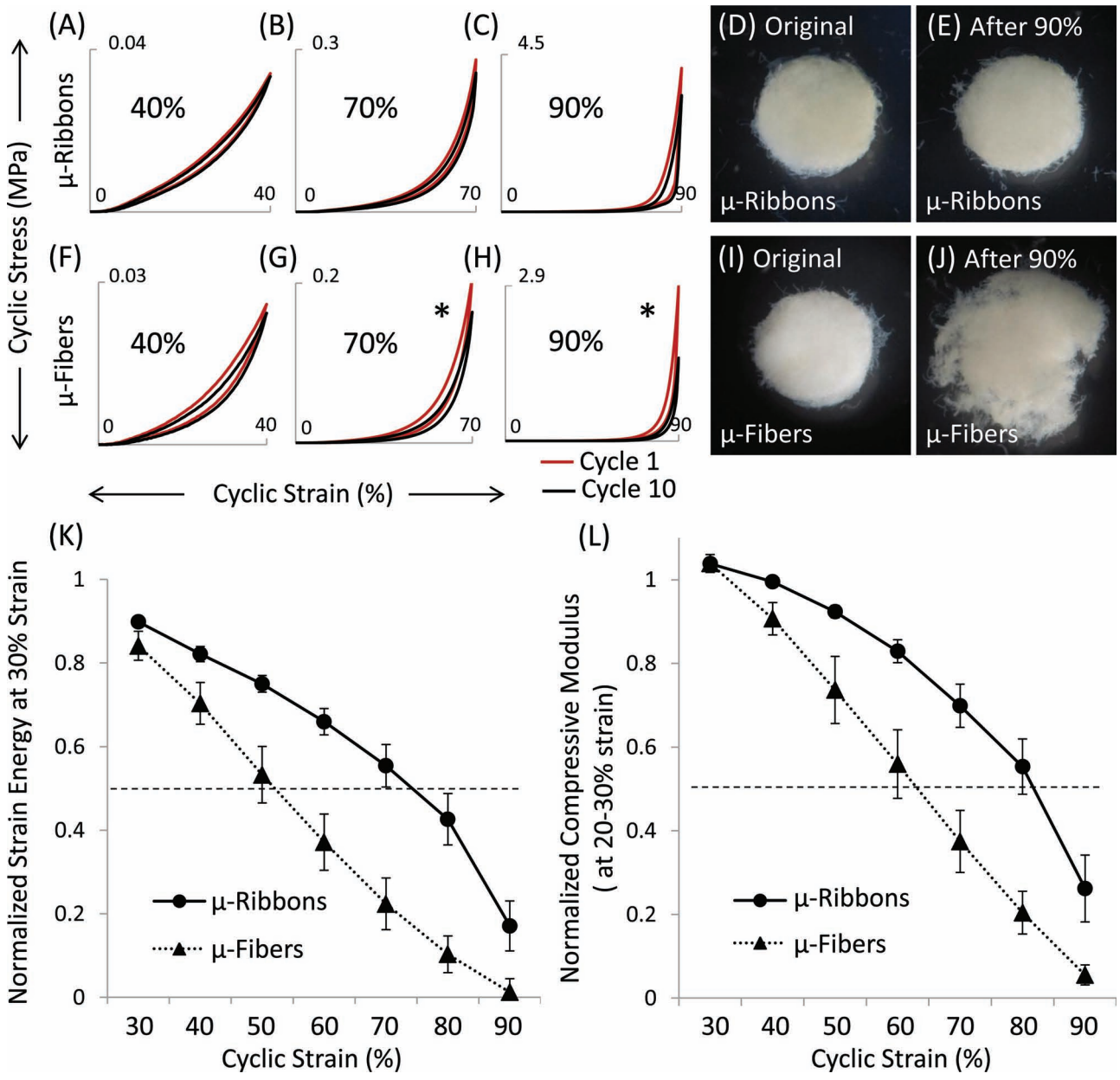

Figure 10. Evaluation of scaffold flexibility. A–C,F–H) Stress responses of microribbon and microfiber-based scaffolds under different cyclic compressions. D,E,I,J) Appearances of microribbon and microfiber-based scaffolds before and after 90% cyclic compressions. K) Changes at 30% strain energy after different cyclic compressions: microribbon vs. microfiber-based scaffolds. L) Changes at compressive modulus (associated with ≈20–30% strain) after different cyclic compressions: microribbon vs. microfiber-based scaffolds.

stress responses using stress-strain data (**Figure 10**). Up to 70% strain level, the microribbon-based scaffolds performed consistent (less than 10% change) stress responses for 10 compression cycles (Figure 10A–C), indicating insignificant damage during the cyclic compressions. In contrast, when the strain level exceeded 40%, the microfiber-based scaffolds showed inconsistent stress responses during the 10 compression cycles (Figure 10F–H), suggesting that substantial damage had taken place.

The damage from cyclic-compression was further measured by the changes in strain energy density, compressive modulus, and scaffold appearance. The microribbon-based scaffolds maintained more than 50% strain energy density (at 30% compression) after being exposed to 70% cyclic compressions, while the microfiber-based scaffolds lost more than 50% strain energy density after being exposed to 60% cyclic compressions (Figure 10K). Furthermore, the microribbon-based scaffold maintained more than 50% compressive modulus (at ≈20–30% strain) after receiving 80% cyclic compressions, while the microfiber-based scaffolds lost more than 50% modulus after receiving 70% cyclic compressions. Visually,

Table 2. Compressive modulus of microribbon vs. microfiber scaffolds (5% w/w) at different strains.

Strain	μ-Ribbon Scaffold [kPa]	μ-Fiber Scaffold [kPa]
0–10%	26.1 ± 4.1	23.2 ± 10.6
10–20%	59.3 ± 10.0	50.7 ± 18.3
20–30%	92.5 ± 12.3	91.8 ± 33.1
30–40%	155.5 ± 20.3	161.7 ± 57.7
40–50%	289.7 ± 33.6	294.5 ± 94.3
50–60%	593.6 ± 50.3	576.2 ± 176.7
60–70%	1518.6 ± 123.3	—[a)]
70–80%	6795.3 ± 516.7	—
80–90%	35 615.1 ± 4142.9	—

[a)]The microfiber-based scaffold falls apart when the strain exceeds 60%.

the microribbon-based scaffolds reversed to their original shapes (Figure 10D,E) after receiving 90% cyclic-strain, while the microfiber-based scaffolds gradually fell apart as the cyclic-strain level exceeded 60% (Figure 10I,J).

To our knowledge, such exceptional flexibility and resilience of the microribbon-based scaffolds has not been previously reported on any other microfiber-based scaffolds, most of which comprise symmetric cross-section microfibers and lack the similar capacity to absorb stress and deformation. The flexibility of microribbon-based scaffold also significantly surpasses that of typical hydrogel scaffolds, which often undergo mechanical failure at a much lower strain rate (<50%).

As the compression on microribbon-based scaffold increased up to 90%, the microribbon density increased drastically, and the compressive modulus of the microribbon scaffold increased non-linearly from about 20 kPa to 35,600 kPa (or 35.6 MPa) (**Table 2**). This strain-induced hardening and the range of modulus change covers the stiffness range of many tissue types including nerve (≈30 kPa), skin (0.4–0.9 MPa), artery (0.1–1 MPa), and articular cartilage (1–20 MPa).[30–33] Thus the microribbons may be suitable for engineering a broad range of tissue types, from the soft and highly elastic tissues to load-bearing hard tissues. Since flexibility are highly desirable for engineering shock-absorbing tissues, these microribbon-based scaffolds could be particularly useful for engineering cartilage tissues, such as intervertebral disc, meniscus, and articular cartilage.[34–37]

3. Conclusion

In conclusion, here we report the development of a novel, microribbon-based scaffold with exceptional mechanical flexibility that facilitates cell growth and tissue formation in 3D. The interconnected macroporosity of the microribbons support cells adhesion, spreading and alignment, leading to cell proliferation by up to 30 fold within 3 weeks. Cellular responses and mechanical properties of the microribbon-based scaffold can be tuned easily by varying fabrication parameters including the wet-spinning rate, drying temperature, choice of drying agent, level of pre-fixation, and the density of microribbons. The scaffold formed by the microribbons can sustain up to 90% strain and 3 MPa stress without failing, and such exceptional flexibility and resilience would provide a particularly useful scaffold for engineering shock-absorbing tissues such as cartilage and spines.

4. Experimental Section

Materials: Type-A gelatin, dimethyl sulfoxide, methacrylic anhydride, glutaraldehyde, and L-lysine hydrochloride were purchased from Sigma-Aldrich (St. Louis, MO). Photoinitiator Irgacure 2959 (Ir2959) was received from Ciba Specialty Chemistry (Basel, Switzerland). All chemicals were used as received.

Synthesizing the Gelatin Microribbons by Wet-Spinning: To prepare a spinnable solution, type-A gelatin (GelA) (5g) was stirred in 23 mL dimethyl sulfoxide (DMSO) (23 mL) at 40 °C for 12 h, forming a viscous solution of GelA. To carry out the wet-spinning process that produces microribbons from GelA, the GelA/DMSO solution was transferred into a 20-mL syringe pump and was ejected trough 16-gauge needle at adjustable rate (5 or 10 mL per h) by the pump at room temperature into a tank of anhydrous ethanol (4L), which was situated 6 feet under the syringe outlet and stirred by a 5-cm long magnet at 1100 rpm. In the ethanol tank the stream of GelA was promptly dried and turned into a cluster of microfibers. The microfibers were collected and transferred into acetone, and were dried in acetone for 3 h at either 25 or 60 °C. The as-formed microribbons were washed 3 times by ethanol and then dissociated in ethanol into short segments (<1 mm in length) using a homogenizer.

Methacrylation and Fixation of the Gelatin Microribbons: To integrate methacrylate groups, which enable photocrosslinking, the as-formed microribbons were stirred at 25 °C for 3 h in a mixture of methacrylic anhydride (20 mL) and methanol (100 mL). The methacrylated microribbons were transferred to a solution of 0.1% glutaraldehyde in methanol (200 mL) and were vigorously stirred at 40 °C for either 3 or 12 h. The aldehyde-fixed microribbons were washed 3-times with DI water and neutralized at 25 °C for 12 h in a solution of 1% L-lysine hydrochloride in phosphate buffered saline (PBS) (200 mL). The microribbons were finally washed 5 times with 25 °C DI water, freeze-dried, and were stored at –20 °C before use.

Photocrosslinking of Microribbons and the Formation of Highly Porous Scaffolds: To prepare a scaffold precursor, the freeze-dried microribbons were rehydrated in PBS containing Ir-2959 (50 mg mL^{-1}), at a microribbon density of 25–100 mg per mL. Following 1 h of incubation at 25 °C, the precursor was transferred to a polypropylene molding (5.6 mm in diameter and 3 mm in height) which was designed to give the scaffolds a cylindrical shape. The molded precursor was exposed to a source of ultraviolet (UV) light (365 nm, 4mW cm^{-2}) for 5 min, such exposure caused the crosslinking among microribbons, producing a highly-porous scaffold of sponge-like physical quality.

Measurement of Scaffold Volume: The volumes of microribbon scaffolds were measured after photocrosslinking and were measured again after the scaffolds were incubated for 48 h in 37 °C PBS. The diameter (D) and thickness (t) of each scaffold were measured with 0.1 mm precision using a caliber, the scaffold volume (V) was calculated by: $V = \frac{1}{4}\pi D^2 t$.

Scanning Electron Microscopy: The morphology of hydrated microribbon-based scaffolds was assessed using a Hitachi S-3400N variable pressure scanning electron microscope (VP-SEM). Samples were incubated in PBS at 37 °C overnight and rinsed with DI water before being loaded to the chamber of SEM. The hydrated samples were gradually cooled from room temperature to –25 °C as the chamber pressure reduced from 1 atm to 50 Pa, following a P/T curve at which water stays liquid phase. The samples were imaged under the electron beam intensity at 15 kV and a working distance around 7 mm.

Isolation and Culturing of Human Adipose Derived Stromal Cells: Human adipose derived stromal cells (hADSCs) were isolated from lipoaspirated

human fat tissue as previously described.[38] All the procedure involving human tissue has been approved by the Stanford Institutional Review Board. The fat tissues were washed 2–3 times with PBS and digested at 37 °C for 30 min with Blendzyme 3 (Roche Diagnostics, Indianapolis, IN) (0.5 U mL^{-1}). Enzyme activity was neutralized with Dulbecco's modified Eagle medium (DMEM), containing fetal bovine serum (FBS, Invitrogen) (10%) and antibiotic penicillin/streptomycin (P/S) solution (1%). The cells were then filtered through a 70 μm cell strainer to remove cellular debris, counted and seeded onto tissue culture flasks. Following the initial 48 h of incubation at 37 °C and 5% CO_2, cells were washed with PBS and expanded in DMEM with 10% FBS, 1% P/S and 10 ng mL^{-1} of basic fibroblast growth factor (bFGF) (PeproTech, Rocky Hill, NJ). Cells were passaged upon 85–90% confluence and passage 3 cells were used for all experiments.

Cell Spreading on Microribbons: On day 0, the microribbons of different types were rehydrated at a low density (1 mg mL^{-1}) by PBS containing Ir2959 (0.05%), and were exposed to UV light (365 nm, 4 mW cm^{-2}) for 5 min, causing individual microribbons to self-crosslink but remain separated. The microribbons were then transferred to a 24-well plate at a density of 10 mg per well, and each well was seeded with hADSCs at a density of 10 000 cells per well. On day 1, 4, 10, and 16, the microribbons were sampled and attached cells were stained using LIVE/DEAD Viability/Cytotoxicity Kit for mammalian cells (Invitrogen). Cell morphology on the microribbons were imaged using fluorescence microscopy and analyzed using Image J (n = 300). Cell-spreading was quantified by the area of hADSCs, and cell-alignment was quantified by the sharp angles between the long-axes of cells and the center-line of microribbons underneath the cells.

Cell Proliferation in Crosslinked Microribbon Scaffolds: Trypsinized hADSCs were gently suspended with microribbons precursor at cell density of 5 million per mL. To create scaffolds with controlled thickness to facilitate cell imaging, precursor were molded between two glass slides (with gap of 0.25 mm in between). Upon exposing to UV light (365 nm, 4 mW cm^{-2}, 5 min), the cell-laden microribbons crosslinked into a thin sheet (0.25 mm thick) of scaffold. Following the initial 24 h of incubation (37 °C, 5% CO_2), the cell-laden scaffolds were cut into circular samples and transferred to 96-well plates. To visualize cell proliferation over time, cell-laden scaffolds were stained using live/dead staining and imaged using fluorescent microscopy. To quantify cell proliferation, samples were collected (n = 3) on day 1, 6, 13, and 20 and cell number was determined using CellTiter 96 AQueous One Solution Cell Proliferation Assay (Promega, Carlsbad, CA). Each sample was incubated in a mixture of CellTiter-96 (20 μL) and culture medium (100 μL) for 2 hours, after which medium was collected and medium absorbance was measured at 490 nm using a SpectraMax-M2e microplate reader (Molecular Devices, Sunnyvale, CA).

Mechanical Testing: Unconfined compression tests were conducted using an Instron 5944 materials testing system (Instron Corporation, Norwood, MA) fitted with a 10 N load cell (Interface Inc., Scottsdale, Az). The test set-up consisted of custom made aluminum compression platens lined with PTFE to minimize friction. All tests were conducted in PBS solution at room temperature. Before each test, the scaffold's diameter (≈4.5 mm) and thickness (≈2.5 mm) were measured using digital calipers A preload of approximately 2 mN was applied to ensure the scaffold surface was in full contact with the upper platen. To measure compressive modulus, the upper platen was lowered at a rate of 1% strain per second to a maximum strain of 15%. Load and displacement data were recorded at 100 Hz. Stress vs. strain curves were created and curve fit using a third order polynomial equation. The compressive modulus of scaffold was determined from the curve fit equation at strain values of 5%, 10%, and 15%.

Flexibility Evaluation: To evaluate scaffold flexibility, cyclic compressions were applied to the microribbon-based and microfiber-based scaffolds (5 wt%) at strain levels of 30, 40, 50, 60, 70, 80, and 90 percents. For each strain level, scaffolds (n = 5) were compressed and released for ten cycles at the rate of 5% s^{-1}. The loading and displacement data was recorded at 10 Hz, and for each compression cycle the strain energy density (in J m^{-3}) at 30% strain was calculated numerically using the following equation ($US_{30\%}$: strain energy density at 30% strain, σ: stress, ε: strain):

$$US_{30\%} = \int_0^{0.3} \sigma(\varepsilon) \mathrm{d}\varepsilon \quad (1)$$

The change (decrease) at $US_{30\%}$was associated with the damage at scaffold networks upon cyclic compressions, and thus $US_{30\%}$was used as the indicator of scaffold flexibility: the scaffolds with less-decreased $US_{30\%}$upon cyclic loading were considered more flexible and resilient. In addition to quantitative measurements, scaffold flexibility was also evaluated visually based on the scaffolds' structure integrity upon cyclic compressions.

Statistical Analysis: All data were expressed as mean ± standard error and statistical significance was determined by analysis of variance using student's t-test with equal variance. p values (two-tails) of less than 0.05 were considered statistically significant, and p values less than 0.005 were considered statistically highly significant.

Supporting Information

Supporting Information is available from the Wiley Online Library or from the author.

Acknowledgements

This work has been disclosed to the Office Technology Licensing at Stanford University. The authors would like to thank the Donald E. and Delia B. Baxter Foundation, the McCormick Faculty Award, and Stanford Bio-X Interdisciplinary Initiative grant for funding.

Received: May 3, 2012
Revised: July 17, 2012
Published online: September 4, 2012

[1] E. Cukierman, R. Pankov, D. R. Stevens, K. M. Yamada, *Science* **2001**, *294*, 1708.
[2] T. Jacks, R. A. Weinberg, *Cell* **2002**, *111*, 923.
[3] A. Abbott, *Nature* **2003**, *424*, 870.
[4] J. Debnath, K. R. Mills, N. L. Collins, M. J. Reginato, S. K. Muthuswamy, J. S. Brugge, *Cell* **2002**, *111*, 29.
[5] K. A. Mosiewicz, K. Johnsson, M. P. Lutolf, *J. Am. Chem. Soc.* **2010**, *132*, 5972.
[6] C. A. DeForest, B. D. Polizzotti, K. S. Anseth, *Nat. Mater.* **2009**, *8*, 659.
[7] C. J. Flaim, S. Chien, S. N. Bhatia, *Nat. Methods* **2005**, *2*, 119.
[8] Y. Soen, A. Mori, T. D. Palmer, P. O. Brown, *Mol. Syst. Biol.* **2006**, *2*, 37.
[9] J. A. Benton, B. D. Fairbanks, K. S. Anseth, *Biomaterials* **2009**, *30*, 6593.
[10] O. Jeon, K. H. Bouhadir, J. M. Mansour, E. Alsberg, *Biomaterials* **2009**, *30*, 2724.
[11] J. W. Nichol, S. T. Koshy, H. Bae, C. M. Hwang, S. Yamanlar, A. Khademhosseini, *Biomaterials* **2010**, *31*, 5536.
[12] J. D. Hartgerink, E. Beniash, S. I. Stupp, *Science* **2001**, *294*, 1684.
[13] M. Ma, Y. Kuang, Y. Gao, Y. Zhang, P. Gao, B. Xu, *J. Am. Chem. Soc.* **2010**, *132*, 2719.
[14] J. Rnjak, Z. Li, P. K. Maitz, S. G. Wise, A. S. Weiss, *Biomaterials* **2009**, *30*, 6469.
[15] C. P. Fik, M. Meuris, U. Salz, T. Bock, J. C. Tiller, *Adv. Mater.* **2011**, *23*, 3565.
[16] R. J. DeVolder, H. Bae, J. Lee, H. Kong, *Adv. Mater.* **2011**, *23*, 3139.

[17] S. Y. Chew, R. Mi, A. Hoke, K. W. Leong, *Adv. Funct. Mater.* **2007**, *17*, 1288.
[18] R. A. Barry, R. F. Shepherd, J. N. Hanson, R. G. Nuzzo, P. Wiltzius, J. A. Lewis, *Adv. Mater.* **2009**, *21*, 2407.
[19] K. D. Nelson, A. Romero, P. Waggoner, B. Crow, A. Borneman, G. M. Smith, *Tissue Eng.* **2003**, *9*, 1323.
[20] S. J. Hollister, *Nat. Mater.* **2005**, *4*, 518.
[21] A. I. Van Den Bulcke, B. Bogdanov, N. De Rooze, E. H. Schacht, M. Cornelissen, H. Berghmans, *Biomacromolecules* **2000**, *1*, 31.
[22] H. Wang, M. B. Hansen, D. W. Lowik, J. C. van Hest, Y. Li, J. A. Jansen, S. C. Leeuwenburgh, *Adv. Mater.* **2011**, *23*, H119.
[23] A. Ovsianikov, A. Deiwick, S. Van Vlierberghe, P. Dubruel, L. Moller, G. Drager, B. Chichkov, *Biomacromolecules* **2011**, *12*, 851.
[24] a) M. Rumpler, A. Woesz, J. W. Dunlop, J. T. van Dongen, P. Fratzl, *J. R. Soc., Interface* **2008**, *5*, 1173; b) N. Gjorevski, C. M. Nelson, *Integr. Biol.* **2010**, *2*, 424.
[25] J. L. Gornall, E. M. Terentjev, *Phys. Rev. Lett.* **2007**, *99*, 028304.
[26] D. Eagland, G. Pilling, R. G. Wheeler, *Faraday Discuss. Chem. Soc.* **1974**, 181.
[27] a) Y. Hong, J. Guan, K. L. Fujimoto, R. Hashizume, A. L. Pelinescu, W. R. Wagner, *Biomaterials* **2010**, *31*, 4249; b) M. J. Mondrinos, R. Dembzynski, L. Lu, V. K. Byrapogu, D. M. Wootton, P. I. Lelkes, J. Zhou, *Biomaterials* **2006**, *27*, 4399; c) V. J. Chen, P. X. Ma, *Biomaterials* **2004**, *25*, 2065.
[28] D. E. Discher, P. Janmey, Y. L. Wang, *Science* **2005**, *310*, 1139.
[29] A. J. Engler, S. Sen, H. L. Sweeney, D. E. Discher, *Cell* **2006**, *126*, 677.
[30] K. Hirakawa, K. Hashizume, T. Hayashi, *No To Shinkei* **1981**, *33*, 1057.
[31] P. G. Agache, C. Monneur, J. L. Leveque, J. De Rigal, *Arch. Dermatol. Res.* **1980**, *269*, 221.
[32] H. Hasegawa, H. Kanai, Y. Koiwa, *IEEE Trans. Ultrason. Ferroelectr. Freq. Control* **2004**, *51*, 93.
[33] G. Bellucci, B. B. Seedhom, *Rheumatology (Oxford)* **2001**, *40*, 1337.
[34] Y. Shikinami, Y. Kotani, B. W. Cunningham, K. Abumi, K. Kaneda, *Adv. Funct. Mater.* **2004**, *14*, 1039.
[35] C. J. Spaans, V. W. Belgraver, O. Rienstra, J. H. de Groot, R. P. Veth, A. J. Pennings, *Biomaterials* **2000**, *21*, 2453.
[36] B. M. Baker, R. P. Shah, A. H. Huang, R. L. Mauck, *Tissue Eng., Part A* **2011**, *17*, 1445.
[37] N. L. Nerurkar, B. M. Baker, S. Sen, E. E. Wible, D. M. Elliott, R. L. Mauck, *Nat. Mater.* **2009**, *8*, 986.
[38] P. A. Zuk, M. Zhu, H. Mizuno, J. Huang, J. W. Futrell, A. J. Katz, P. Benhaim, H. P. Lorenz, M. H. Hedrick, *Tissue Eng.* **2001**, *7*, 211.